Accepted Manuscript

A novel photoelectrochemical immunosensor by integration of nanobody and ZnO nanorods for sensitive detection of Nucleoside diphosphatase kinase-A

Anran Liu, Kaifei Yin, Li Mi, Mengyao Ma, Yuanjian Liu, Ying Li, Wei Wei, Yuanjian Zhang, Songqin Liu

PII: S0003-2670(17)30402-6

DOI: 10.1016/j.aca.2017.03.048

Reference: ACA 235149

To appear in: *Analytica Chimica Acta*

Received Date: 21 October 2016

Revised Date: 24 February 2017

Accepted Date: 24 March 2017

Please cite this article as: A. Liu, K. Yin, L. Mi, M. Ma, Y. Liu, Y. Li, W. Wei, Y. Zhang, S. Liu, A novel photoelectrochemical immunosensor by integration of nanobody and ZnO nanorods for sensitive detection of Nucleoside diphosphatase kinase-A, *Analytica Chimica Acta* (2017), doi: 10.1016/j.aca.2017.03.048.

This is a PDF file of an unedited manuscript that has been accepted for publication. As a service to our customers we are providing this early version of the manuscript. The manuscript will undergo copyediting, typesetting, and review of the resulting proof before it is published in its final form. Please note that during the production process errors may be discovered which could affect the content, and all legal disclaimers that apply to the journal pertain.

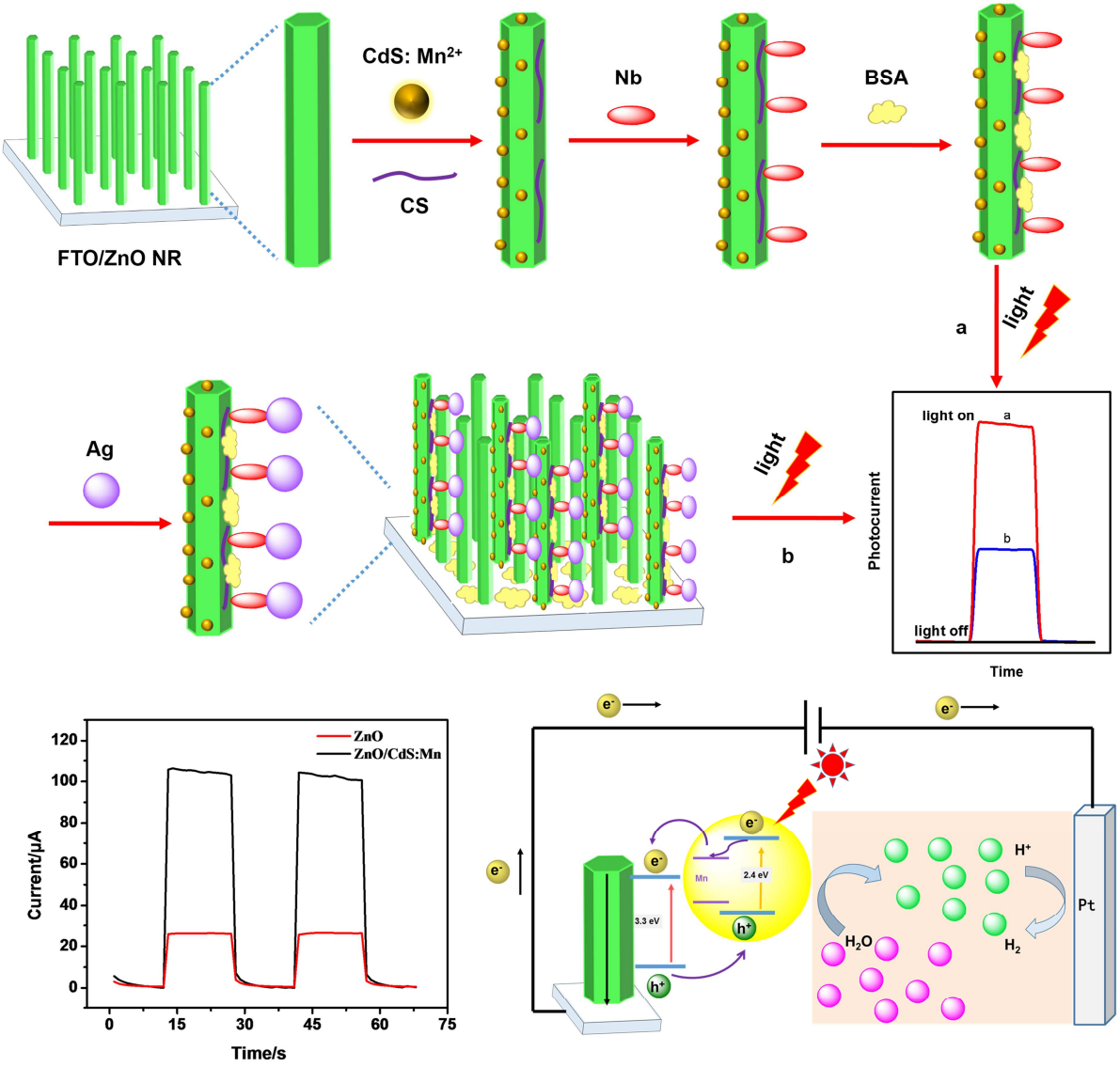

ACCEPTED MANUSCRIPT

ACCEPTED MANUSCRIPT

A novel photoelectrochemical immunosensor by integration of nanobody and ZnO nanorods for sensitive detection of Nucleoside diphosphatase kinase-A

Anran Liu*, Kaifei Yin, Li Mi, Mengyao Ma, Yuanjian Liu, Ying Li, Wei Wei, Yuanjian Zhang and Songqin Liu

Corresponding Author

*E-mail: liuar@seu.edu.cn

Jiangsu Engineering Laboratory of Smart Carbon-Rich Materials and Device (CMD), Jiangsu Province Hi-Tech Key Laboratory for Bio-medical Research, School of Chemistry and Chemical Engineering, Southeast University, Nanjing, 211189, P. R. China

ACCEPTED MANUSCRIPT

ACCEPTED MANUSCRIPT

Abstract. Nucleoside diphosphatase kinase A (NDPK-A) is a metastasis-suppressor protein and a biomarker that act on a wide range cancer cells to inhibit the potential metastasis. Herein, we present a simple photoelectrochemical immunosensor based on ZnO nanorod arrays for the sensitive detection of NDPK-A. The ZnO nanorod arrays cosensitized with CdS nanoparticles and Mn^{2+} displayed a high and stable photocurrent response under irradiation. After anti-NPDK-A nanobodies were immobilized to the ZnO nanorod arrays, the proposed immunosensor can be utilized for detecting NPDK-A by monitoring the changes in the photocurrent signals of the electrode resulting from immunoreaction. Accordingly, the well-designed immunosensor exhibited a low limit of detection (LOD) of 0.3 pg mL^{-1} and a wide linear range from 0.5 pg mL^{-1} to 10 μg mL^{-1}. The R^2 of the regression curve is 0.99782. Meanwhile, the good stability, reproducibility and specificity of the resulting photoelectrochemical biosensor are demonstrated. In addition, the presented work would offer a novel and simple approach for the detection of immunoreactions and provide new insights in popularizing the diagnosis of NPDK-A.

Keywords: ZnO nanorod; photoelectrochemical immunosensor; nanobody; NDPK-A

ACCEPTED MANUSCRIPT

1. Introduction

Nucleoside diphosphatase kinase-A (NDPK-A) is encoded by the NM23 gene (non-metastasis 23rd), which is associated with propensity and severity of all kinds of tumor cells[1-5]. Recent research demonstrate that NDPK-A is a metastasis-suppressor protein that act on a wide range cancer cells to inhibit the potential metastasis[6]. Moreover, the expression of NDPK-A shows positive correlation with the deterioration of lung cancer [7] and non-hodgkin lymphoma (NHL[8]). It is obviously overexpressed in hematologic neoplasms than normal blood cells[9]. The high level of NDPK-A in plasma indicates a poor prognosis[10]. Although NDPK-A plays an important role in metastasis and oncogenesis, no other effective method except enzymelinked immunosorbent assay (ELISA) has been found for accurate detection of NDPK-A[11]. Despite there are many merits of ELISA, it's still limited by elevated background signals, low sensitivity and relative high LOD. Besides, although introducing enzyme as a label could amplify the detection signal, yet it also complicated the operating procedure, which increased the time and cost simultaneously. To this end, it is essential and emergency to establish a new label-free method, which is ultrasensitive, simple and low-cost, for quantitative determination of NDPK-A.

Photoelectrochemical (PEC) immunosensors have developed rapidly in recent years[12-14]. The PEC detection signal is independent of the excitation source, reducing the undesired background noises significantly[15]. PEC immunosensors are also label-free, which makes the experimental processes time-saving and low-cost [16]. In a typical PEC immunosensor, an antibody is immobilized onto the surface of an electrode. By measuring the photocurrent response after the specific immunoreaction between the antibody and antigen (analyte) of different concentrations, the correlation between the photocurrent and the concentration of the analyte can be determined. Apparently, optoelectronic material plays the role of soul during the construction of PEC sensors. Among various kinds of photoactive materials, ZnO is widely used because of its high performance in chemical stability and biocompatibility. Additionally, under the appropriate condition, it qualified be fashioned into all sorts of shapes within nano-scale, such as particle[17], schistose[18], flowerlike[19], siphonate[20], and rods[21] et.al. One–dimensional structure (1D) like tubes or rods are quite beneficial for PEC signal amplification[22-23], for the reason that 1D structure is more in favor of electron transfer via micrometer-scale axial length while in the meantime enable facilitate the charge separation effectively across the nanometer-scale diameter[24]. Nonetheless, the ZnO has obvious drawbacks limiting its application in PEC, for ZnO with a wide band gap can only absorb the UV light, which restricts the efficiency of photon-to-charge process[25]. Therefore, it is highly promising to assemble a cosensitized structure that is composed of a wide band gap semiconductor and a photosensitizer whose band gap is relative smaller and CB is low potential.

Nanobodies (Nbs), also termed as Variable domains of heavy-chain antibodies (VHH) [26], is a unique type of conventional antibody fragment and naturally in the serum of camelidae. It is the smallest known antigen-binding antibody fragment (~15 kD)[27], and has aroused a progressively attention in

ACCEPTED MANUSCRIPT
immunosensor for higher binding specificity and greater thermal stability[28-29], with hydrophilic residue substitutions in the framework-two region, it demonstrates a more soluble ability and a lower tendency for aggregation than conventional antibody[30]. With these benefits, Nbs are more suitable than normal antibodies in the next fluorescent competitive immunosensors.

Herein, we report a label-free and sensitive PEC immunosensor for NDPK-A based on anti-NDPK-A nanobody immobilization method. In this work, a ZnO nanorod arrays/CdS:Mn cosensitized structure was utilized to detect the immunoreactions between antibody and antigen. To test the performance of the immunosensor, samples with different concentrations of NDPK-A were introduced and the photocurrent signal changes were recorded. This PEC immunosensor exhibited high sensitivity, stability, reproducibility and specificity.

2. **Experimental Section**

2.1. Materials and Reagents

The fluorine-doped tin oxide (FTO) conductive glass were purchased from Zhuhai Kaivo Electronic Components Co., Ltd. (sheet resistance <15 ohm sq^{-1}, China).3-aminopropyl triethoxysilane(APTES), Chitosan powder (CS)，Bovine serum albumin（BSA）were all obtained from Sigma−Aldrich(USA). Glutaraldehyde (GA, 25% aqueous solution) was purchased from Alfa Aesar(USA). Hexamethyleneteramine (HTM) was obtained from Aladdin (China). Zinc acetate（$Zn(CH_3COO)_2$, zinc nitrate（$Zn(NO_3)_2$），manganese acetate ($Mn(AC)_2$)，Cadmium nitrate（$Cd(NO_3)_2$），sodium sulfide（Na_2S），were purchased from Sinopharm Chemical Reagent Co., Ltd. (China). Anti-NDPK was purchased from Millipore (USA). Human chorionic gonadotropin (HCG), prostate-specific antigen (PSA) and α-fetoprotein (AFP) were obtained from Shanghai Ruiqi Biological Technology Co., Ltd. (Shanghai, China). Unconjugated oestriol antigen (uE3) were purchased from Abcam, Inc. (America). The anti-NDPK-A nanobodies were provided by Pro Y.K.Wan (Shanghai Institute of Materia Medica, Chinese Academy of Sciences). All other reagents were of analytical grade and were used as received. All aqueous solutions were prepared with deionized water (DI water, 18.2 MΩ/cm, Thermal, USA)

2.2. Apparatus

UV−*vis* absorption spectroscopy was taken on a Cary series 100 UV−vis spectrophotometer (Agilent, Singapore). The photoluminescence (PL) spectra were performed by fluorescence spectrometer (Fluoromax-4, Horiba Jobin Yvon, Japan). Morphology and size of the ZnO nanorods and ZnO/CdS:Mn electrodes et.al were examined on Ultra Plus field-emission scanning electron microscopy (SEM, Zeiss, Germany) and Transmission electron microscopy (TEM) images were measured on a JEM-2100 field-emission electron microscope (JEOL, Japan) at an acceleration voltage of 200 kV. Energy dispersive X-ray spectra (EDX) were taken on Ultra Plus field-emission scanning electron microscope (SEM, Zeiss, Germany). X-ray diffraction (XRD) was performed on a D8 Advance diffractometer equipped with

high-intensity Cu Kα radiation (λ = 1.54178 Å) (Advance, Bruker, Germany), and the data were collected in the 2θ range of 10−90° at a step size of 0.02°.

Determination of photocurrent were carried out with a CHI 660C electrochemical workstation (Chenhua, Shanghai, China) in a conventional three-electrode system in a quartz tank composed of the modified FTO electrode with an area of 0.7 cm^2 as a working electrode, an Ag/AgCl (saturated KCl) electrode as the reference electrode, and a platinum wire as a counterelectrode. A white light Xe lamp source of 150 W (Beijing NBeT Co., Ltd.) was used as the irradiation source. The illuminating light intensity was 1 sun illumination, estimated by a radiometer.

Electrochemical impedance spectroscopy (EIS) was performed on Gamry660 electrochemical workstation(USA) in a 0.1M PBS(PH 7.4) solution containing redox probe, which were 0.1M KCl and $K_3[Fe(CN)_6]/K_4[Fe(CN)_6]$ (2 mM, 1:1) mixture ,with a three-electrode system ,The impedance spectra were recorded at an open circuit potential of 0.2V(vs. SCE) with an amplitude of 10 mV over a frequency range from 0.01 Hz to 100 kHz.

2.3. Preparation of ZnO/CdS:Mn Electrode

The FTO electrode were cut into pieces of 0.7cm × 1cm, and then ultrasonically cleaned in 1M KOH, acetone, ethanol and deionized (DI) water respectively. Well-aligned ZnO nanorod arrays (ZnO NAs) were prepared according to the literature method with appropriate modifications. Firstly, A NaOH solution in methanol (0.03 M) was added slowly to a solution of zinc acetate dihydrate (0.01M) in methanol (V_1:V_2 = 52:100) at 60 °C with intense stirring for 2 hours. The resulting sol is colorless and transparent, and the nanoparticles are spherical and stable for at least one week in solution. Then, the pretreated FTO electrodes were immersed in the zinc oxide sol and quickly pulled out after 10 seconds, following 3 times and then annealed at 150 °C for 1 hour to form seeds. The process was repeated by 5 cycles. Secondly, the FTO substrates with ZnO seeds were placed in sealed teflon reactor, containing 0.025 M $Zn(NO_3)_2$ and 0.025 M hexamethylenetetramine, followed by heating at 95 °C for 2–8 h to grow the oriented ZnO nanorods. The products were washed with DI water several times to dissolve the surfactant and the residual salt and then dried at 60 °C.

In order to obtain the complex of ZnO/CdS:Mn, successive ionic layer adsorption and reaction (SILAR) technique was adopted. The FTO with ZnO nanoroad arrays were dipped into 0.1 M $Cd(NO_3)_2$ mixed with 0.08 M $Mn(Ac)_2$ methanol solution for 2 min, washed with ethanol and then immersed into 0.1M aqueous solution of Na_2S for another 2 min ,again rinsed with ethanol. The above cycles were repeated by 2-16 times. The products were dried at 60°C reserved to use.

2.4. Fabrication of the Photoelectrochemical Immunosensor

The fabrication procedure of the immunosenor is shown in Scheme 1. Briefly, chitosan (CS) solution (0.05 wt %) was prepared by dissolving chitosan powder in 1% acetic acid. Forty microliters of CS solution was dropped onto ZnO/CdS:Mn electrode and dried in air. The ZnO/CdS:Mn/CS electrode was washed with 1 M NaOH and deionized (DI) water, respectively. Then the electrode was silanized by immersing in 10%

ACCEPTED MANUSCRIPT

3-aminopropyl triethoxysilane (APTES) anhydrous ethanol solution overnight. The as-prepared silanized ZnO/CdS:Mn/CS reacted with anti-NDPK-A nanobodies (Nbs) solution (10μg mL^{-1}) via a linker chemistry using a solution of glutaraldehyde (GA 2.5%, 25μL), the resulting electrode was incubated at 4 °C in a moisture atmosphere to avoid solvent evaporation. After incubation for 16h, the electrode was rinsed with PBS (0.01M, PH7.4) thoroughly to remove physically adsorbed Nbs. Subsequently, the electrode was covered with 20 μL of blocking buffer solution(1% BSA in 0.01M PBS, PH 7.4) for 30min at room temperature to block nonspecific binding sites and washed with the PBS thoroughly. The FTO/ZnO/CdS:Mn/CS/APTES/GA/Nbs/BSA electrode (hereafter called ZnO/Nbs electrode) was used as a photoelectrochemical (PEC) immunosensor and incubated in NDPK-A (Antigen, 25 μL) solution with a variety of concentrations for 40 min. Finally, the electrode was rinsed with PBS, and introduced into respective PEC measurement.

2.5. Photoelectrochemical Detection.

The antigen (NDPK-A) was analyzed with the concentration from 5 pg mL^{-1} to 10 mg mL^{-1}, and each concentration of the sample was tested 5 times. The calibration curve was obtained according to linear relationship between the photocurrent difference (ΔI) and the logarithmic value of the NDPK-A concentration. The ΔI means the difference between the ZnO/Nbs electrode before and after being incubated with NDPK-A. Photoelectrochemical detection was carried out at room temperature in PBS (pH 7.4, 0.1 M). Xe lamp was utilized as excitation light at 1 sun illumination and was switched on and off every 15 s. The applied potential was 0.2 V.

2.6. Preparation of Clinical Samples.

Human serum specimens are sampling from healthy donors at the Second Affiliated Hospital of Southeast University, Nanjing, China. The serum was spiked with different concentrations of the target antigen and measured by the same procedure applied for NDPK-A detection above. In order to cover the wide linear detection range of the proposed immunosensor, the serum were used either as received or diluted appropriately with 10 mM phosphate buffer solution (pH 7.4) before assay.

3. **Results and discussion**

3.1. Characterization of ZnO nanorods and FTO/ZnO/CdS:Mn electrode

The ZnO nanorod arrays (ZnO NAs) were synthesized through a two-step hydrothermal process and ZnO /CdS:Mn nano-composites were synthesized by successive ionic layer adsorption and reaction (SILAR) method[31-32].

The as prepared ZnO NAs were highly uniform and vertical to the substrates. The morphology of the ZnO NAs was characterized by scanning electron microscopy (SEM) and transmission electron microscope (TEM). From the top view of sample (Fig.1A), the structure of the ZnO NAs was hexagonal prism with an average diameter of 60-90 nm. The side-view images of the ZnO NAs sample (Fig.S1A) confirmed that all nanorods grown almost perpendicularly from the FTO substrate with a length of 1μm. The hexagonal structure of ZnO nanorods was also demonstrated by X-ray diffraction (XRD) analysis of ZnO nanorods

ACCEPTED MANUSCRIPT

(Fig. S1B). All of the diffraction peaks from the ZnO NAs samples are in good accord with the wurtzite-type ZnO (JCPDS No. 36-1451).

After CdS:Mn deposition, it could be seen that the original smooth nanorod arrays surface(Fig.1B) are almost completely covered with CdS nanoparticles(Fig.1C). According to the TEM image of ZnO/CdS:Mn, the thickness of the CdS shell is estimated to be 10-20nm(Fig.1D) and the size of CdS nanoparticles was estimated to be 15±5 nm. The energy dispersive spectroscopy (EDX) of the ZnO/CdS:Mn electrode shows that the Zn, Cd, S and Mn elements were all homogeneously distributed in the electrode surface(Fig.S2), indicating the successful deposition of CdS particles and Mn^{2+} ions.

3.2. **Photoelectrochemical Properties of the FTO/ZnO/CdS:Mn electrode**

This three-dimensional (3D) nanostructures of ZnO nanorod arrays increased the specific surface area enable loading more biomolecule. The ZnO nanorods can provide fast charge transport through the micrometer-scale axial lengths[33], which constituted a stable photocurrent upon irradiation. All of these are the elements sufficiently affirmed ZnO nanorod arrays is an appropriate choice as the carrier of PEC sensors.

ZnO/CdS: Mn cosensitized structure was used as the PEC matrix for the biosensing electrode. Highly ordered ZnO NAs electrode has photoelectric activity, large surface area, biocompatibility, high stability and low cost, which is suit for PEC detection. However, pure ZnO possesses a wide band gap (about 3.2 eV) and it can only absorb ultraviolet light. The wide band gap and the poor utilization of light energy limit its use in PEC biosensors. Enhancing photocurrent response and reducing electron-hole recombination require combining ZnO with other materials with narrow band gap to form a cosensitized structure[34]. The band gap of CdS is about 2.4 eV[35]. Covering ZnO NAs with CdS can adequately utilize the light energy and significantly promote the photocurrent intensity[36]. Mn^{2+} can be introduced into CdS to form the CdS:Mn doping structure. The lifetime of electron−hole recombination for CdS:Mn^{2+} is hundreds of microseconds which is much longer than that of CdS only (dozens of nanoseconds)[37]. The photocurrent response of FTO/ZnO and FTO/ZnO/CdS:Mn electrode was shown in Fig.2A. Upon irradiation with visible light at 1 sun illumination, the FTO/ZnO electrode showed a photocurrent of 26.18μA at an applied potential of 0.2V, whereas the FTO/ZnO/CdS:Mn electrode possessed a photocurrent of 104.50 μA, which is improved by approximately four times at same conditions. The result was attributed to the improvement of electron transfer via the strong electronic coupling between the excited state of CdS:Mn^{2+} and the conduction band (CB) of ZnO. The photocurrent generation mechanism of the FTO/ZnO/CdS:Mn is illustrated in Fig.2B. To be specific, the lowest CB of CdS is -3.98 eV[38], which lies more negative than the CB level of ZnO (-4.19 eV)[39]. Upon irradiation, the photoinduced electrons would quickly transfer from the CB of CdS to the CB of ZnO and subsequently flow to an external circuit of the PEC system through the conductive FTO substrate. Meanwhile, holes in the ZnO valence band (VB, -7.39 eV) would transfer to the VB (-6.38 eV) of CdS and combine with the electrons from the oxidation of H_2O[38, 39]. Owing to the perfect matching of energy levels between the two semiconductors, the photocurrent intensity was greatly improved.

The combination of ZnO and CdS could expand the range of light absorption, which can be proved by the UV-*vis* spectra of ZnO/CdS. The UV-*vis* spectra of the ZnO, CdS and ZnO/CdS:Mn was shown in Fig.

ACCEPTED MANUSCRIPT

S3A. Since the pure ZnO can only absorb ultraviolet light, achieving the maximum absorption at 359nm. After CdS were deposited, the light absorption range expanded to visible light region. The absorption wavelength of the ZnO/CdS:Mn composites started from 330nm to 500nm, and the peak shifted to 386nm, which indicated a more effective utilization of visible light and increasing photocurrent response. Another reason for the improvement of photocurrent response can be attributed to the decline of radiative transition of the composites which is confirmed by fluorescence spectrum (Fig. S3B). Owing to the heterojunction structure formed by ZnO and CdS:Mn, the original fluorescence emission of ZnO occurring in 383nm was quenched, suggesting the radiative transition of ZnO transformed into the electronic energy, which is beneficial to the enhancement of photocurrent response.

In order to get the maximum photocurrent intensity, the growth time of ZnO nanorods by hydrothermal reaction and the number of SILAR cycles were optimized. Fig.S4A shows the effect of hydrothermal reaction time on photocurrent response. In the beginning, the current was enhanced with the increase of hydrothermal reaction time and reached a peak value when the hydrothermal time is 3 hours. After further increase of the hydrothermal reaction time, the photocurrent intensity gradually reduced. During the early period of ZnO nanorod formation, the ZnO crystal were preferred to grow along with the C axis, which can be confirmed by the 002 peaks in XRD of ZnO (Fig. S1B). At this stage, the growth rate in C axis was faster than that in other orientation and the height of ZnO nanorods increase with the reaction time. After reacting for 3 hours, the growth rate in diameter would exceed the rate in height and the diameter of ZnO nanorods increased obviously with the reaction time, thus reducing the specific surface area of ZnO nanorods. The ZnO nanorods became too thick to transfer electrons. Thus, 3 hours of time is chosen for hydrothermal reaction. The number of SILAR cycles is another important factor for photocurrent intensity. The deposition of CdS:Mn onto FTO/ZnO substrate was carried out by a cycle of two steps: the FTO with ZnO NAs was dipped into 0.1 M $Cd(NO3)_2$ mixed with 0.08 M $Mn(Ac)_2$ methanol solution and then into 0.1M aqueous solution of Na_2S, respectively for 2 min. As shown in the Fig. S4B, the photocurrent response was enhanced with the number of SILAR cycles before 10 cycles. During this stage, more CdS:Mn nanoparticles were deposited onto the ZnO nanorods as the SILAR cycles increased, which enhanced the photocurrent response. After 10 cycles, the photocurrent response decreased as the SILAR cycles increased. It is because the excess CdS:Mn nanoparticles formed on the surface of ZnO would enlarge the diffusion resistance for electron transfer and cause the decline of the photocurrent. Thus, 10 cycles is chosen as the optimized number of SILAR cycles.

3.3. Characterization of the Immunosensor Fabrication.

The construction of the PEC immunosensor is shown in Scheme 1. After FTO/ZnO/CdS:Mn electrode was prepared, chitosan (CS) and (3-aminopropyl) triethoxysilane (APTES) were constructed onto the ZnO/CdS:Mn nanorod arrays to supply amidogen for nanobodies (Nbs) coupling. After that, glutaraldehyde (GA, 2.5%) was employed to crosslink with the NDPK-A specific Nb, and bovine serum albumin (BSA) was used to block the nonspecific binding sites. The as-prepared FTO/ZnO/CdS:Mn/CS/APTES/GA/Nbs/BSA electrode (hereafter called ZnO/Nbs electrode) was used as a

PEC immunosensor.

The construction of the PEC immunsensor is primarily utilized the Strong metal oxide support interaction (SMOSI)[40-41] between the FTO and ZnO, the Vander Waals forces and Hydrogen bond[42] between the CS film and ZnO nanorod arrays. The anti-NDPK-A Nbs were coupled to the animo group of APTES via glutaraldehyde and Nbs that could specifically recognize corresponding antigen.

The SEM, UV-Vis spectra and other characterization such as EDX can be used to judge whether the ZnO/Nbs electrode is successfully fabricated. When the ZnO/CdS:Mn sequentially modified with CS, APTES, Nbs and BSA, it could be found that the whole ZnO nanorod assay nearly connected with each other and form a near-net-like pore structure(Fig.1E), which made a substantial decrease of the photoelectric material's surface area where should been receives illumination , resulting in the decline of the photocurrent. From (Fig.1F) it can be seen that on the modified electrode, there are C, Zn, Si, O, Cd, S, Mn et.al elements, which can partly verify the successful modify of the ZnO/Nbs electrode.

EIS is an effective method to monitor the fabrication process of the PEC immunosensor.[43] As shown in Fig.3A, the Nyquist plots of each electrode involved during every construction step reflect the interface properties of the electrodes. The diameter of the semicircle equals the electron transfer resistance (R_{et}) of the redox probe and reflects the restricted diffusion of the redox probe through the multilayer system related directly to film permeability. Bare FTO electrode exhibited the lowest R_{et} (curve a). After the hydrothermal process, the semiconductor ZnO hindered the electron-transfer between the electrode and redox probe, the FTO/ZnO NAs exhibited a larger semicircle (curve b). After the deposition of CdS and Mn^{2+}, the R_{et} at the liquid-surface interface was further increased, indicating the successful immobilization of CdS and Mn^{2+}. Subsequently, chitosan, APTES, Nbs and BSA were constructed on the surface of ZnO nanorods step by step, and the R_{et} of each related electrode increased correspondingly (curve c to g), owing to the insulating property of chitosan, APTES and protein. Finally, when the NDPK-A was immobilized to the electrodes through the specific binding between the antigen to antibody, the R_{et} increased to more than 10000Ω (insert figure). Due to the elevating hindrance effect and insulating effect introduced by the polymers and proteins, the increasing R_{et} of the electrods suggested a successful formation of ZnO/CdS:Mn/CS/APTES/GA/Nbs/ NDPK-A bioconjugates and stepwise fabrication of the proposed biosensor.

The construction of the immunosensor could also be reflected by the corresponding photocurrent response which was shown in Fig.3B. Upon irradiation with visible light at 1 sun illumination, the bare FTO substrate only exhibited a low photocurrent of 10^{-8}A. After the ZnO nanorods grown on the FTO surface, the photocurrent increased obviously to 26.13×10^{-6}A, indicating the ZnO nanorod array is an ideal photoelectric material for the construction of PEC immunosensor. After CdS:Mn were deposited, the electrode generated a peak photocurrent of 1.04×10^{-4} A which was 3.2 times higher than that of FTO/ZnO electrode. As expected, the successive immobilization of CS, APTES, Nbs, BSA on the electrode reduced the photocurrent gradually. After blocking with BSA, the as-obtained immunosensor was incubated with the antigen NDPK-A and the photocurrent intensity further decreased. Such decreases in photocurrent could be explained by the fact that the protein NDPK-A with large spatial dimensions induced steric hindrances against the diffusion of H_2O to

ACCEPTED MANUSCRIPT
the photogenerated holes on the electrode interface and reduced the light-absorbing area of photosensitive materials such as ZnO and CdS:Mn. As control experiment, the ZnO/Nbs electrode was incubated in 0.1M PBS solution without antigen NDPK-A, the test current is approximate 48 μA which is almost the same as that of the ZnO/Nbs electrode. All of the results demonstrated that the PEC immunosensor is successfully fabricated and can be used to detect NDPK-A quantitatively.

3.4. Quantitative determination of NDPK-A

After NDPK-A were specifically bound with the ZnO/Nbs electrode, the photocurrent response of the electrode decreased and the degree of photocurrent response decrement is related to the concentration of NDPK-A. Thus, a sensitive label-free method for quantitatively detecting NDPK-A can be achieved by tracking the final photocurrent variation to monitor the immunoreaction extent of NDPK-A and Nbs on the biosensor. Fig.3C displayed the typical photocurrent responses of the PEC biosensor in the presence of different concentrations of NDPK-A, whereas Fig.3D shows the derived calibration curve. The decrease in photocurrent is dependent on the concentration of NDPK-A. The variation of photocurrent intensity decreased is linearly proportional to the logarithm of the concentration of NDPK-A in the range from 0.5 pg mL^{-1} to 10 μg mL^{-1}. The regression equation was $\Delta I=22.382+5.947 \log C_{Ag}$ (ng mL^{-1}), with the correlation coefficient of 0.99782. The limit of detection (LOD) is 0.3 pg mL^{-1} (S/N=3). The limit of quantification (LOQ) is 0.99 pg mL^{-1} (S/N=10).

3.5. Stability, Reproducibility, Specificity and Real-Sample Analysis.

Stability of the proposed immunosensor was investigated by two tests. After the ZnO/Nbs electrode was incubated with 10ng mL^{-1} NDPK-A, a 800s test of photocurrent response was taken. As shown in Fig.4A, there is no obvious fluctuation during the 800s test, indicating that the biosensor is stable enough for the whole process of PEC detection. The long-time storage stability of the proposed immunosensor was also investigated. The ZnO/Nbs electrode was stored in a dark and moist atmosphere environment at 4°C for over for different periods before the PEC detection of 10ng mL^{-1} NDPK-A. As shown in Fig.4B, 89% of the initial signal was still remained after stored for over 4 weeks, which illustrated the good storage stability and its value in practical applications.

The reproducibility and precision of the proposed immunoassay was estimated by both intra-assay and interassay relative standard deviation (RSD). Analyzed from the testing results with five parallel determinations, the intra-assay RSDs were 2.3%, 3.4%, and 3.7% toward 0.05, 0.5, and 5 ng mL^{-1} of target antigen (NDPK-A), respectively. The interassay RSDs of 2.9%, 3.9%, and 3.4% were acquired by detecting the same samples with five electrodes fabricated independently under identical experimental conditions. These results suggested a satisfactory reproducibility and precision of this immunoassay.

Since specificity is a serious problem hinder the development of the biosensor, because it's difficult to distinguish the nonspecific adsorption from specific binding, which affect the sensitivity and accuracy of the detection results. In order to confirm that the photoelectron signal variation is originated from specific reaction between the antigen and antibody, specificity experiment was investigated by comparing the result response in the same condition with some representative antigen instead of NDPK-A, such as HCG, PSA,

ACCEPTED MANUSCRIPT

AFP, uE3 and their mixture with NDPK-A. The concentration of the rest antigen is 100ng mL^{-1}, which is 10 times higher than the target antigen (10 ng mL^{-1}). The results were displayed in the Fig.4C. As expected, after rinsing with PBS, the electrode incubated with the rest antigen exhibited a low response of photocurrent, and the value is similar to the current of probe incubated in a solution only containing PBS. Comparing with the target antigen, the current difference (ΔI) is low to the extent that could be ignored, even if the concentration is 10 times. When 10 ng NDPK-A were added to the mixture of four different interfering antigen, no significant difference could be found contrast to the response obtained in the presence of 10 ng mL^{-1} only. All the results declared that the immunosensor is high selectivity and stable enough for NDPK-A detection, what's better, it shows a potential in practical application.

Finally, a significant and challenging factor for NDPK-A analysis is the applicability in complex biological matrixes. 100 μL standardized human serum (diluted in 1:10 ratio with the PBS buffer) samples spiked with 0.03, 0.1, 3, 10 and 200 ng NDPK-A respectively and were analyzed with the proposed method. Each concentration of the sample was tested 5 times. The results were shown in Table 1 and exhibited good recoveries varied in the range of 95.7% to 108.1%. The relative standard derivations (RSD) were from 3.42% to 6.35%, indicating that our method had high precision and good reliability for detection of NDPK-A in real examinations and held great potential for clinical analysis.

4. Conclusions

In this work, we developed a label-free photoelectrochemical immunosensors for sensitive NDPK-A determination via specific binding between NDPK-A and anti-NDPK-A Nbs which were immobilized on ZnO NAs electrode. The ZnO NAs displayed a high and stable photocurrent response under irradiation due to their large surface area and ordered nano-architecture. The photocurrent response was improved by the consensitizing ZnO NAs with CdS nanoparticles and Mn^{2+}, as the result of the perfect matching of energy levels between ZnO and CdS, expanding absorption of light energy, fast electron transfer, and effective inhibition of charge recombination. After immobilization of anti-NDPK-A Nbs on the ZnO/Nbs electrode surface, a highly sensitive PEC immunosensor with a broad detection range and a low detection limit (0.3pg mL^{-1}) has been achieved, which also reveals high specificity to NDPK-A. What's more, comparing with conventional detection methods, the PEC biosensor based on nanobodies exhibited longer shelf life, more accuracy in test and more relaxed operating environment, which offers a tremendous advance in immunoassay and provide the possibility of clinical NDPK-A diagnosis.

Supporting Information

Additional information as noted in Supporting Information text.

Notes

The authors declare no competing financial interest.

ACCEPTED MANUSCRIPT

Acknowledgements

This work was financially supported by the National Natural Science Foundation of China (21505018), the Natural Science Foundation of Jiangsu Province of China (BK 20141348) and Fundamental Research Funds for the Central Universities.

ACCEPTED MANUSCRIPT

References

(1) A. De La Rosa, P.S. Steeg, R.L. Williams, Nm23/nucleoside diphosphate kinase: Toward a structural and biochemical understanding of its biological functions, BioEssays, 17 (1995) 53-62.

(2) M. Brune, J.E.T. Corrie, M.R. Webb, A fluorescent sensor of the phosphorylation state of nucleoside diphosphate kinase and its use to monitor nucleoside diphosphate concentrations in real time, Biochemis, 40 (2001) 5087-5094.

(3) C. Charpin, S. Garcia, P. Bonnier, F. Martini, L. Andrac, N. Horschowski, M.-N. Lavaut, C. Allasia, Prognostic significance of nm23/ndpk expression in breast carcinoma, assessed on 10-year follow-up by automated and quantitative immunocytochemical assays, J Pathol, 184 (1998) 401-407.

(4) L. Di, S. Srivastava, O. Zhdanova, Y. Sun, Z. Li, E.Y. Skolnik, Nucleoside diphosphate kinase b knock-out mice have impaired activation of the k+ channel kca3.1, resulting in defective t cell activation, J Biol Chem, 285 (2010) 38765-38771.

(5) J.D. Lapek, G. Tombline, A.E. Friedman, Mass spectrometry detection of histidine phosphorylation on nm23-h1, J Proteome Res, 10 (2011) 751-755.

(6) N. Ishikawa, N. Shimada, Y. Takagi, Y. Ishijima, M. Fukuda, N. Kimura, Molecular evolution of nucleoside diphosphate kinase genes: Conserved core structures and multiple-layered regulatory regions, J Bioenerg and Biomembr, 35 (2003) 7-17.

(7) Y.-S. Hsieh, Y.-L. Lee, S.-F. Yang, J.-S. Yang, W. Chen, S.-C. Chen, C.-M. Shih, Association of ecori polymorphism of the metastasis-suppressor gene nme1 with susceptibility to and severity of non-small cell lung cancer, Lung Cancer, 58 (2007) 191-195.

(8) D.N.T. Aryee, I. Simonitsch, I. Mosberger, K. Kos, G. Mann, E. Schlogl, U. Potschger, H. Gadner, T. Radaszkiewicz, H. Kovar, Variability of nm23-h1/ndpk-a expression in human lymphomas and its relation to tumour aggressiveness, Brit J Cancer, 74 (1996) 1693-1698.

(9) Y.-T. Tee, G.-D. Chen, L.-Y. Lin, J.-L. Ko, P.-H. Wang, Nm23-h1: A metastasis-associated gene, Taiwan J Obstet Gyne, 45 (2006) 107-113.

(10) S. Qu, J. Long, Q. Cai, X.-O. Shu, H. Cai, Y.-T. Gao, W. Zheng, Genetic polymorphisms of metastasis suppressor gene NME1 and breast cancer survival, Clin Cancer Res, 14 (2008) 4787-4793.

(11) D.N.T. Aryee, T. Ströbel, K. Kos, M. Salzer-Kuntschik, A. Zoubek, M. Veron, I.M. Ambros, F. Traincart, H. Gadner, H. Kovar, High nm23-h1/ndpk-a expression in ewing tumors: Paradoxical immunohistochemical reactivity and lack of prognostic significance, Int J Cancer, 64 (1995) 104-111

(12) R. Li, Y. Liu, L. Cheng, C. Yang, J. Zhang, Photoelectrochemical aptasensing of kanamycin using visible light-activated carbon nitride and graphene oxide nanocomposites, Anal Chem, 86 (2014) 9372-9375.

(13) W.-W. Zhao, Z.-Y. Ma, P.-P. Yu, X.-Y. Dong, J.-J. Xu, H.-Y. Chen, Highly sensitive photoelectrochemical immunoassay with enhanced amplification using horseradish peroxidase induced biocatalytic precipitation on a cds quantum dots multilayer electrode, Anal Chem, 84 (2012) 917-923.

(14) X. Zeng, S. Ma, J. Bao, W. Tu, Z. Dai, Using graphene-based plasmonic nanocomposites to quench energy from quantum dots for signal-on photoelectrochemical aptasensing, Anal Chem, 85 (2013) 11720-11724.

ACCEPTED MANUSCRIPT

(15) M. Zhao, G.-C. Fan, J.-J. Chen, J.-J. Shi, J.-J. Zhu, Highly sensitive and selective photoelectrochemical biosensor for hg^{2+} detection based on dual signal amplification by exciton energy transfer coupled with sensitization effect, Anal Chem, 87 (2015) 12340-12347.

(16) Q. Shen, L. Han, G. Fan, J.-R. Zhang, L. Jiang, J.-J. Zhu, "Signal-on" photoelectrochemical biosensor for sensitive detection of human t-cell lymphotropic virus type ii DNA: Dual signal amplification strategy integrating enzymatic amplification with terminal deoxynucleotidyl transferase-mediated extension, Anal Chem, 87 (2015) 4949-4956.

(17) G.-J. Chang, S.-Y. Lin, J.-J. Wu, Room-temperature chemical integration of zno nanoarchitectures on plastic substrates for flexible dye-sensitized solar cells, Nanoscale, 6 (2014) 1329-1334.

(18) W. Li, P. Sheng, J. Cai, H. Feng, Q. Cai, Highly sensitive and selective photoelectrochemical biosensor platform for polybrominated diphenyl ether detection using the quantum dots sensitized three-dimensional, macroporous zno nanosheet photoelectrode, Biosens Bioelectron, 61 (2014) 209-214.

(19)J. Li, G. Lu, Y. Wang, Y. Guo, Y. Guo, A high activity photocatalyst of hierarchical 3d flowerlike zno microspheres: Synthesis, characterization and catalytic activity, J Colloid and Interf Sci, 377 (2012) 191-196.

(20) G. Sun, Y. Zhang, Q. Kong, X. Zheng, J. Yu, X. Song, Cuo-induced signal amplification strategy for multiplexed photoelectrochemical immunosensing using cds sensitized zno nanotubes arrays as photoactive material and aupd alloy nanoparticles as electron sink, Biosens Bioelectron, 66 (2015) 565-571.

(21) D. Liu, L. Wang, S. Ma, Z. Jiang, B. Yang, X. Han, S. Liu, A novel electrochemiluminescent immunosensor based on cds-coated zno nanorod arrays for hepg2 cell detection, Nanoscale, 7 (2015) 3627-3633.

(22) Y. Tang, L. Luo, Z. Chen, Y. Jiang, B. Li, Z. Jia, L. Xu, Electrodeposition of zno nanotube arrays on tco glass substrates, Electrochem Commun, 9 (2007) 289-292.

(23) Z. Kang, Y. Gu, X. Yan, Z. Bai, Y. Liu, S. Liu, X. Zhang, Z. Zhang, X. Zhang, Y. Zhang, Enhanced photoelectrochemical property of zno nanorods array synthesized on reduced graphene oxide for self-powered biosensing application, Biosens Bioelectron, 64 (2015) 499-504.

(24) J. Tang, B. Kong, Y. Wang, M. Xu, Y. Wang, H. Wu, G. Zheng, Photoelectrochemical detection of glutathione by iro2–hemin–tio2 nanowire arrays, Nano Lett, 13 (2013) 5350-5354.

(25) M. Izaki, R. Chizaki, T. Saito, K. Murata, J. Sasano, T. Shinagawa, Hybrid zno/phthalocyanine photovoltaic device with highly resistive zno intermediate layer, ACS Appl Mater Inter, 5 (2013) 9386-9395.

(26) H. Wang, G. Li, Y. Zhang, M. Zhu, H. Ma, B. Du, Q. Wei, Y. Wan, Nanobody-based electrochemical immunoassay for ultrasensitive determination of apolipoprotein-a1 using silver nanoparticles loaded nanohydroxyapatite as label, Anal Chem, 87 (2015) 11209-11214.

(27) J. Wang, Z. Majkova, C.R.S. Bever, J. Yang, S.J. Gee, J. Li, T. Xu, B.D. Hammock, One-step immunoassay for tetrabromobisphenol a using a camelid single domain antibody–alkaline phosphatase fusion protein, Anal Chem, 87 (2015) 4741-4748.

(28) J. Cabanas-Danés, E.D. Rodrigues, E. Landman, J. van Weerd, C. van Blitterswijk, T. Verrips, J. Huskens, M. Karperien, P. Jonkheijm, A supramolecular host–guest carrier system for growth factors employing vhh fragments, J Am Chem Soc, 136 (2014) 12675-12681.

(29) L. Ma, Y. Sun, X. Kang, Y. Wan, Development of nanobody-based flow injection chemiluminescence

ACCEPTED MANUSCRIPT
immunoassay for sensitive detection of human prealbumin, Biosens Bioelectron, 61 (2014) 165-171.

(30) T. He, Y. Wang, P. Li, Q. Zhang, J. Lei, Z. Zhang, X. Ding, H. Zhou, W. Zhang, Nanobody-based enzyme immunoassay for aflatoxin in agro-products with high tolerance to cosolvent methanol, Anal Chem, 86 (2014) 8873-8880.

(31) B. Zhang, J. Zheng, X. Li, Y. Fang, L.-W. Wang, Y. Lin, F. Pan, Tuning band alignment by cds layers using a silar method to enhance tio2/cds/cdse quantum-dot solar-cell performance, Chem Commun, 52 (2016) 5706-5709.

(32) R. Nakamura, S. Makuta, Y. Tachibana, Electron injection dynamics at the silar deposited cds quantum dot/tio2 interface, J Phys Chem C, 119 (2015) 20357-20362.

(33) Q. Li, X. Sun, K. Lozano, Y. Mao, Facile and scalable synthesis of “caterpillar-like” zno nanostructures with enhanced photoelectrochemical water-splitting effect, The J Phys Chem C, 118 (2014) 13467-13475.

(34) A. Torabi, V.N. Staroverov, Band gap reduction in zno and zns by creating layered zno/zns heterostructures, J Phys Chem Lett, 6 (2015) 2075-2080.

(35) G. Sun, Y. Zhang, Q. Kong, C. Ma, J. Yu, S. Ge, M. Yan, X. Song, Chemiluminescence excited paper-based photoelectrochemical competitive immunosensing based on porous zno spheres and cds nanorods, J Mater Chem B, 2 (2014) 7679-7684.

(36) Z. Wang, J. Wang, T.-K. Sham, S. Yang, Origin of luminescence from zno/cds core/shell nanowire arrays, Nanoscale, 6 (2014) 9783-9790.

(37) G.-C. Fan, L. Han, H. Zhu, J.-R. Zhang, J.-J. Zhu, Ultrasensitive photoelectrochemical immunoassay for matrix metalloproteinase-2 detection based on cds:Mn/cdte cosensitized tio2 nanotubes and signal amplification of sio2@ab2 conjugates, Anal Chem, 86 (2014) 12398-12405.

(38) Q. Shen, J. Jiang, S. Liu, L. Han, X. Fan, M. Fan, Q. Fan, L. Wang, W. Huang, Facile synthesis of au-sno2 hybrid nanospheres with enhanced photoelectrochemical biosensing performance, Nanoscale, 6 (2014) 6315-6321.

(39) A. Yousef, N.A.M. Barakat, S.S. Al-Deyab, R. Nirmala, B. Pant, H.Y. Kim, Encapsulation of cdo/zno nps in pu electrospun nanofibers as novel strategy for effective immobilization of the photocatalysts, Colloid Surfaces A, 401 (2012) 8-16.

(40) X. Liu, M.-H. Liu, Y.-C. Luo, C.-Y. Mou, S.D. Lin, H. Cheng, J.-M. Chen, J.-F. Lee, T.-S. Lin, Strong metal–support interactions between gold nanoparticles and zno nanorods in co oxidation, J Am Chem Soc, 134 (2012) 10251-10258.

(41) P. Kast, M. Friedrich, F. Girgsdies, J. Kröhnert, D. Teschner, T. Lunkenbein, M. Behrens, R. Schlögl, Strong metal-support interaction and alloying in pd/zno catalysts for co oxidation, Catal Today, 260 (2016) 21-31.

(42) Z. Li, Y. Du, Z. Zhang, D. Pang, Preparation and characterization of cds quantum dots chitosan biocomposite, React Funct Polym, 55 (2003) 35-43.

(43) H. Li, Y. Mu, J. Yan, D. Cui, W. Ou, Y. Wan, S. Liu, Label-free photoelectrochemical immunosensor for neutrophil gelatinase-associated lipocalin based on the use of nanobodies, Anal Chem, 87 (2015) 2007-2015.

ACCEPTED MANUSCRIPT

Scheme 1. Schematic representation of construction process of the PEC immunosensor.

Figure.1. SEM image (A) and TEM image (B) of the FTO/ZnO NAs; SEM image (C) and TEM image (D) of FTO/ZnO/Cds:Mn electrode; SEM image (E) of FTO/ZnO/CdS:Mn/CS/APTES/Nbs/BSA electrode and (F) the corresponding EDX analysis.

Figure.2. (A) Photocurrent intensity of FTO/ZnO NAs and FTO/ZnO/Cds:Mn electrode and (B) Mechanism of photocurrent generation and electron-hole transfer in the FTO/ZnO/Cds:Mn PEC System.

Figure. 3. Nyquist plots of EIS (A) and the corresponding photocurrent responses (B) of the electrodes: (a)bare FTO, (b)FTO/ZnO, (c)FTO/ZnO/CdS:Mn, (d)FTO/ZnO/CdS:Mn/CS, (e)FTO/ZnO/CdS:Mn/CS/APTES, (f)FTO/ZnO/CdS:Mn/CS/APTES/Nbs, (g)FTO/ZnO/CdS:Mn/CS/APTES/Nbs/BSA, (h)FTO/ZnO/CdS:Mn/CS/APTES/Nbs/BSA/Ag. (C) Photocurrent responses and (D) corresponding calibration curve of the PEC immunosensor in the presence of different concentrations of NDPK–A from 0.5 pg mL^{-1} to 10μg mL^{-1}. The ΔI is the difference between the PEC immunosensor before and after being incubated with NDPK-A. The insert function is the linear relationship between the photocurrent difference (ΔI) and the logarithmic value of the NDPK-A concentration. R^2 represents the correlation coefficient.

Figure.4. Stability test of the PEC immunosensor via photocurrent response of detection probe incubated with 10ng/ml NDPK-A (A) in a PEC test of 800s and (B) a PEC test during four weeks. (C) The selectivity test by comparing the ΔI of 10ng mL^{-1} target Ag with the interfering antigen (100 ng mL^{-1}) and the mixed solution. ΔI is the photocurrent difference between the detection probe before and after the incubation with NDPK-A or interfering antigen respectively.

Table 1. Recovery results of NDPK-A added in real samples

Scheme 1

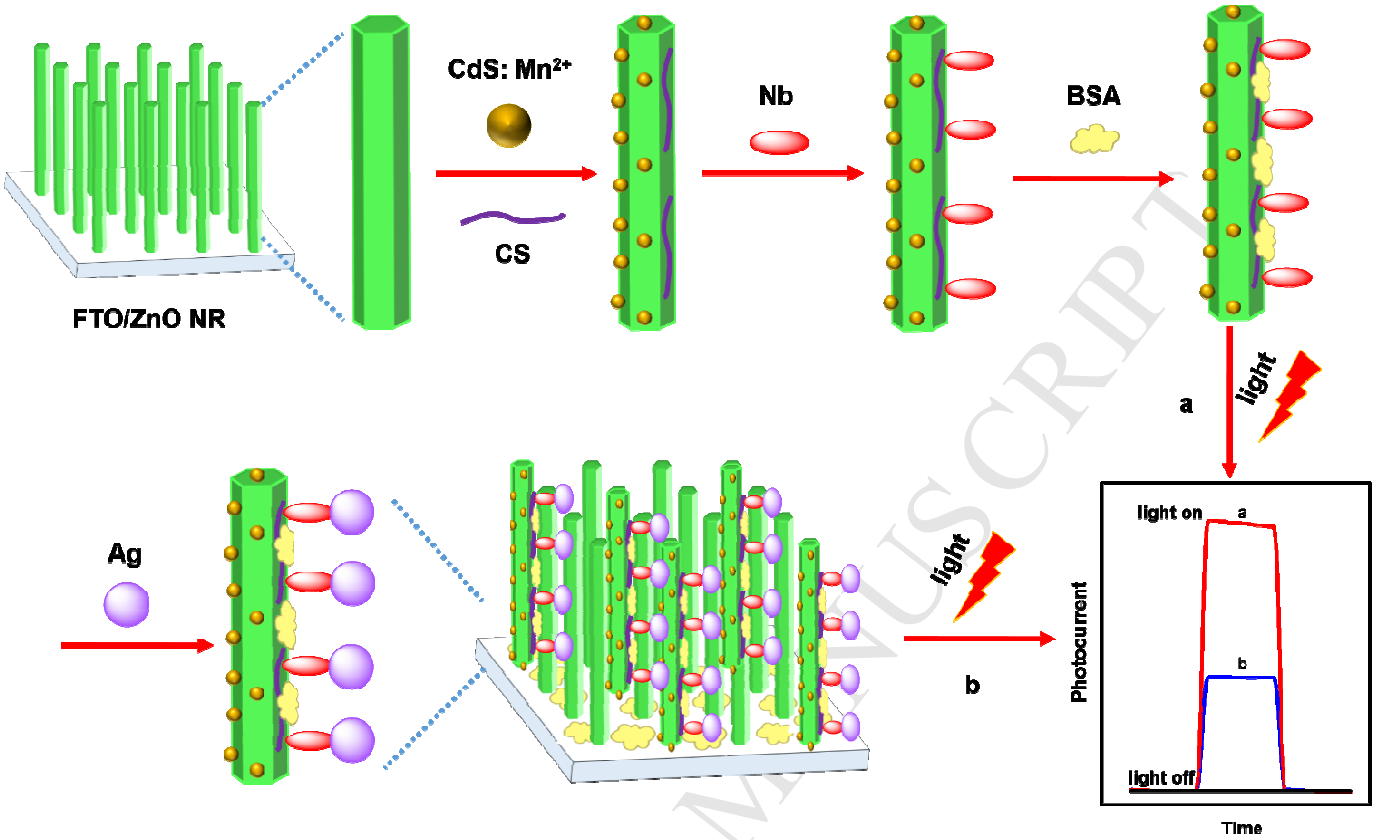

ACCEPTED MANUSCRIPT

Fig.1

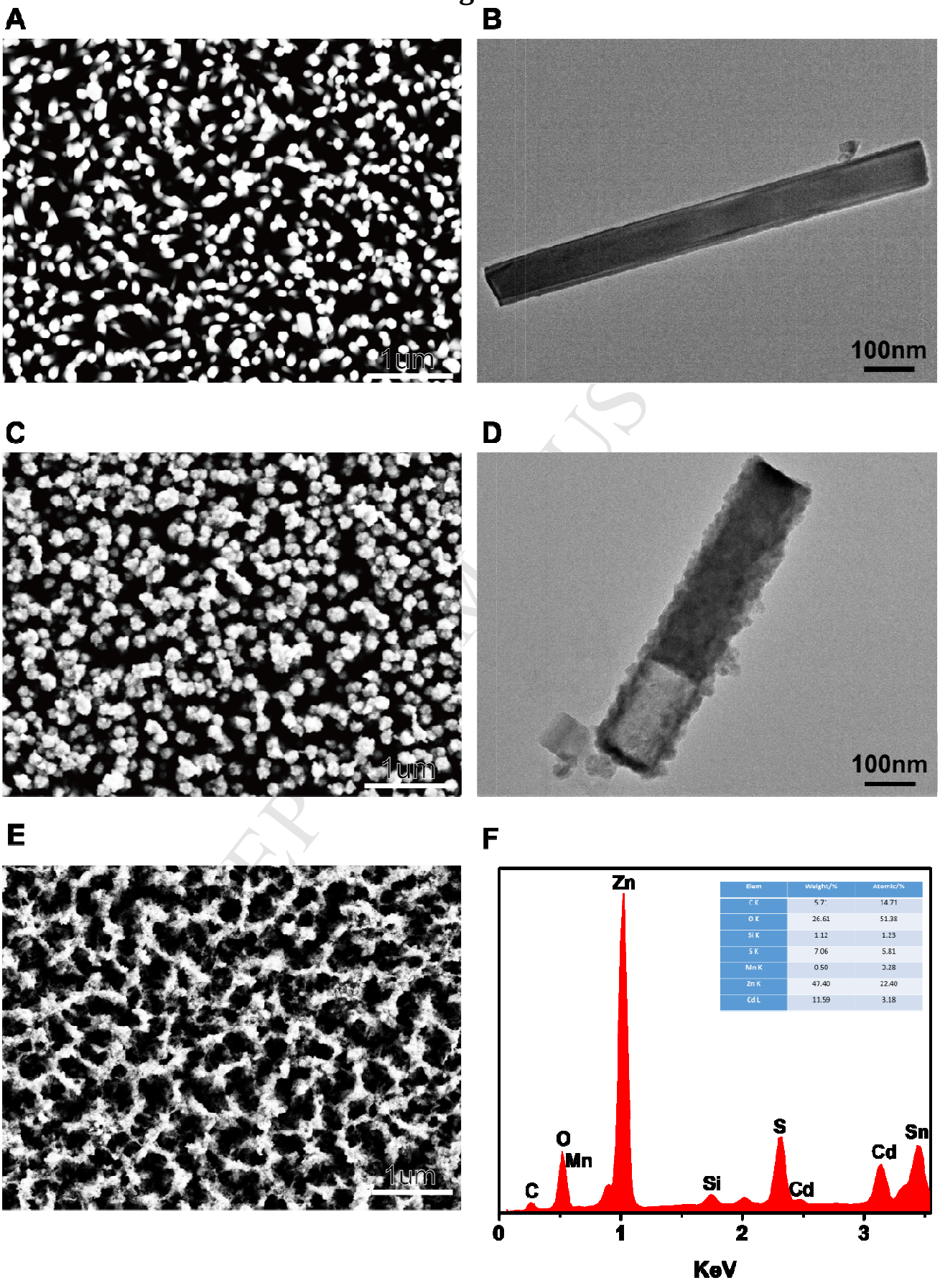
A
B
1um
100nm
C
D
1um
100nm
E
F
1um
Zn
O
Mn
C
Si
S
Cd
Cd
Sn
0
1
2
3
KeV
Elem Weight/% Atomic/%
C K 5.7 14.71
O K 26.61 51.38
Si K 1.12 1.23
S K 7.06 5.81
Mn K 0.50 0.28
Zn K 47.40 22.40
Cd L 11.59 3.18

Fig.2

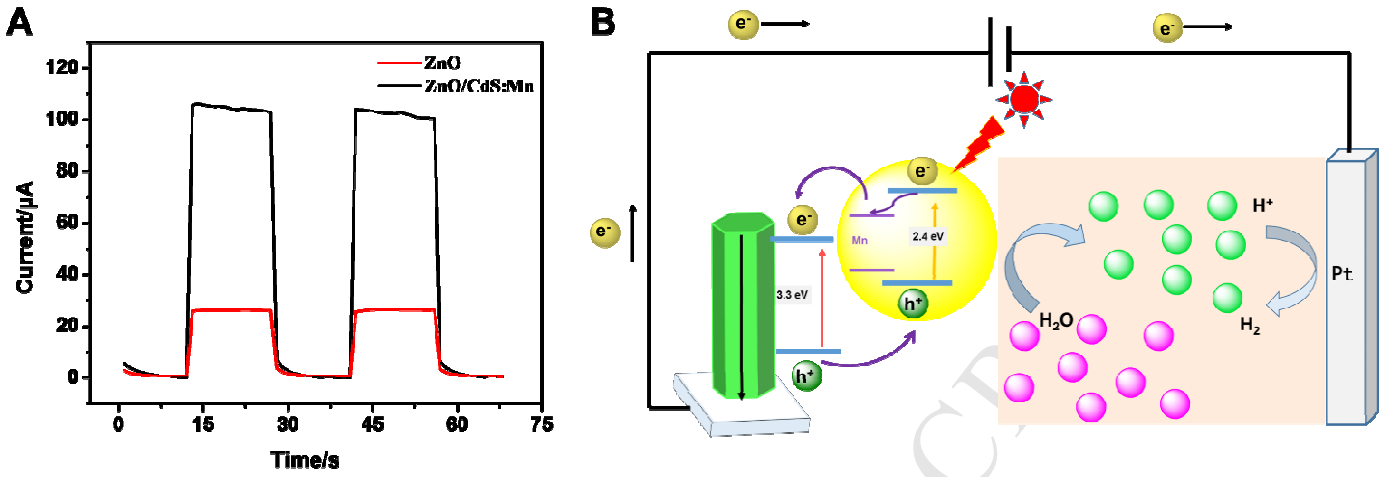

ACCEPTED MANUSCRIPT

Fig.3

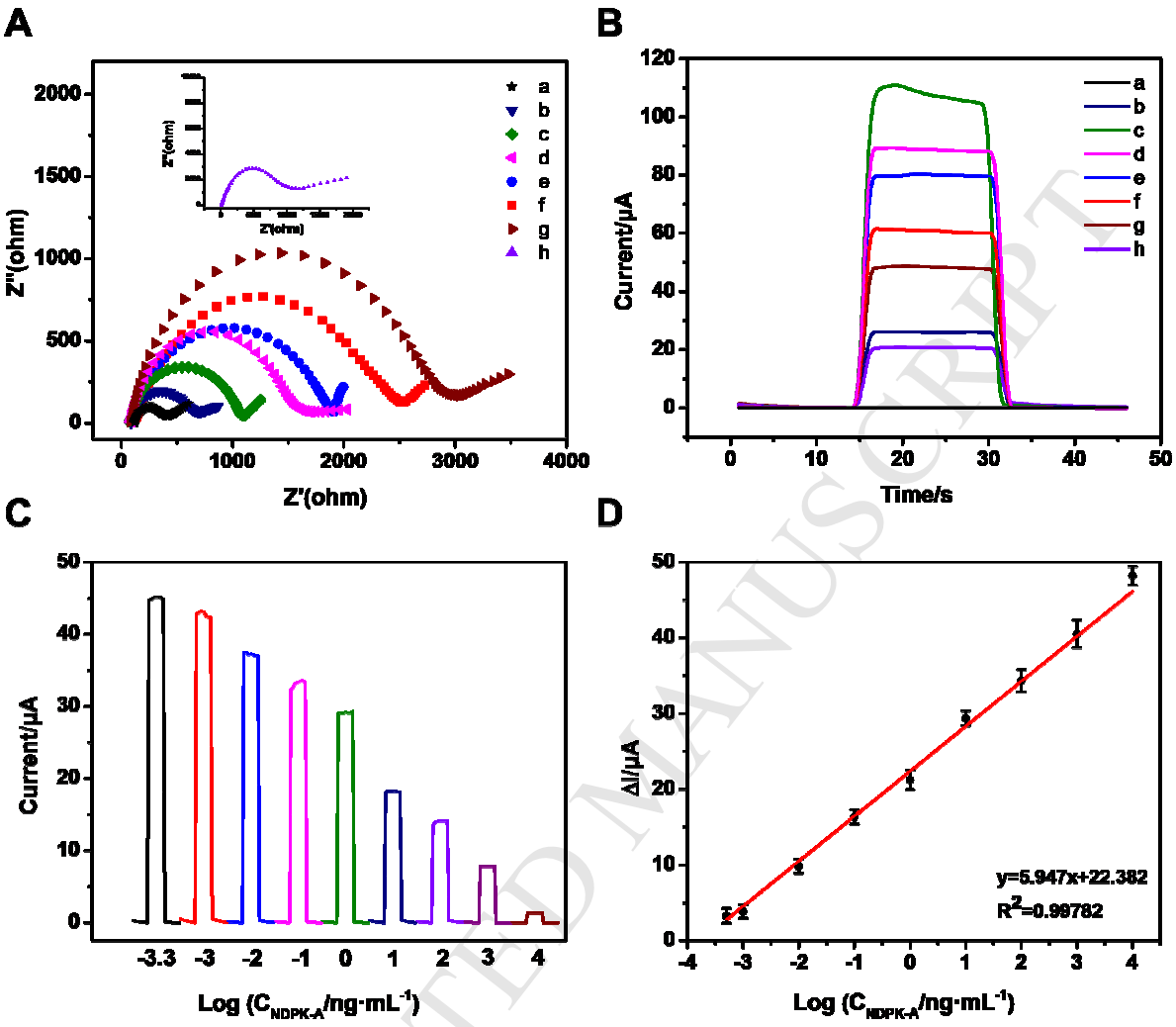

ACCEPTED MANUSCRIPT

Fig.4

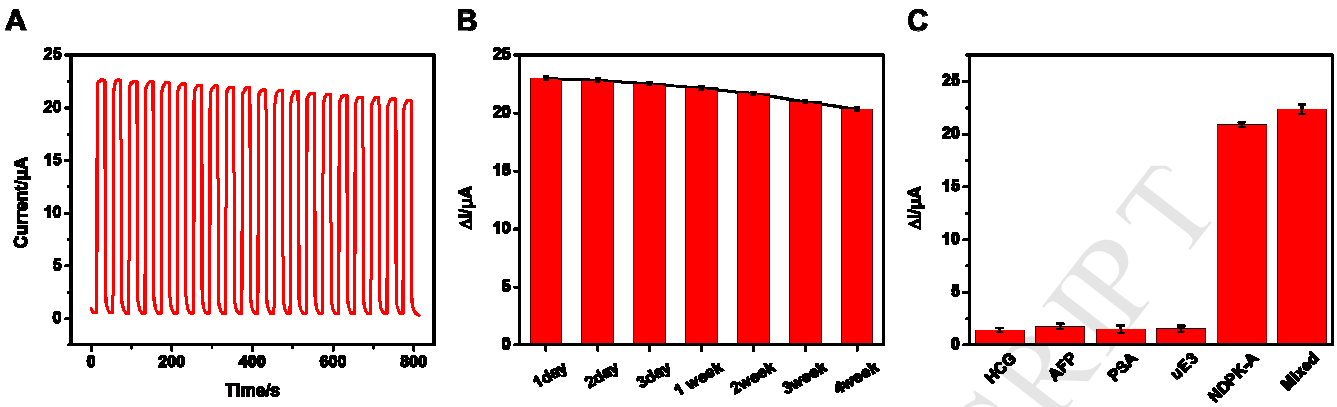

ACCEPTED MANUSCRIPT

Table 1. Recovery Results of NDPK-A Added in Real Samples

Sample No.	Added(ng mL^{-1})	Found(ng mL^{-1})	Recovery (%)	RSD(%,n=5)
1	0	--	--	--
2	0.03	0.029	95.7	6.35
3	0.1	0.11	106.0	5.72
4	3	3.24	108.1	3.98
5	10	10.05	104.5	3.42
6	200	197.97	98.99	4.17

ACCEPTED MANUSCRIPT

ACCEPTED MANUSCRIPT

Table 1. Recovery Results of NDPK-A Added in Real Samples

Sample No.	Added(ng mL^{-1})	Found(ng mL^{-1})	Recovery (%)	RSD(%,n=5)
1	0	--	--	--
2	0.03	0.029	95.7	6.35
3	0.1	0.11	106.0	5.72
4	3	3.24	108.1	3.98
5	10	10.05	104.5	3.42
6	200	197.97	98.99	4.17

ACCEPTED MANUSCRIPT

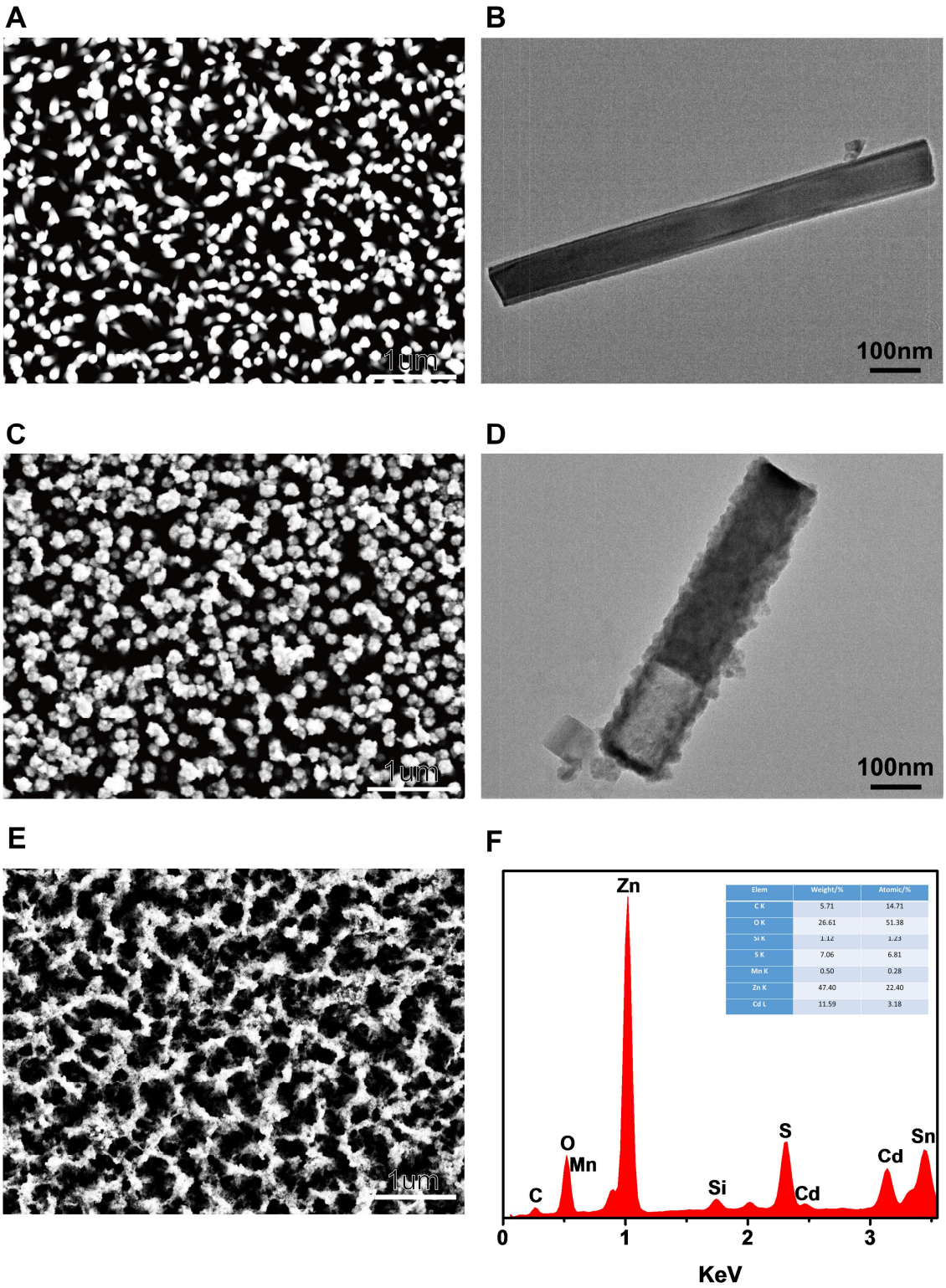
A
1um
B
100nm
C
1um
D
100nm
E
1um
F
Zn
O
Mn
C
Si
S
Cd
Cd
Sn
0
1
2
3
KeV
Elem Weight/% Atomic/%
C K 5.71 14.71
O K 26.61 51.38
Si K 1.12 1.23
S K 7.06 6.81
Mn K 0.50 0.28
Zn K 47.40 22.40
Cd L 11.59 3.18

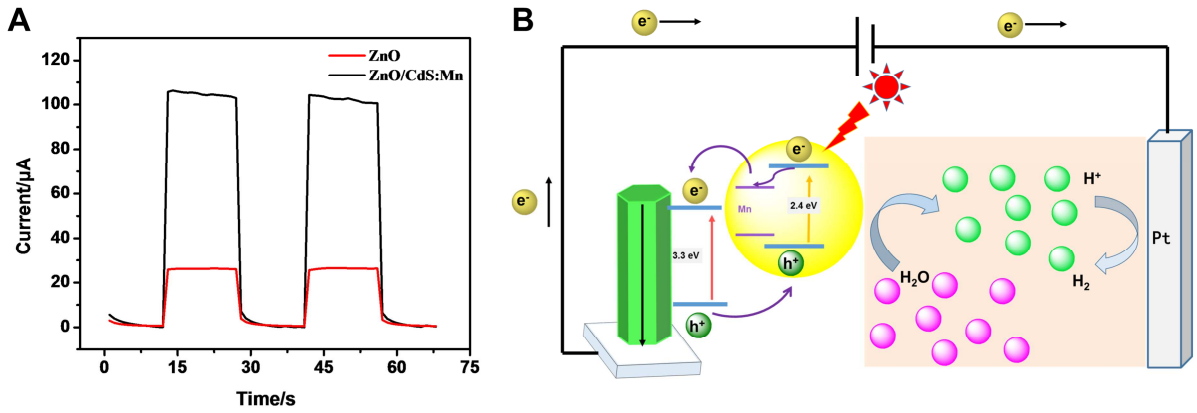

ACCEPTED MANUSCRIPT

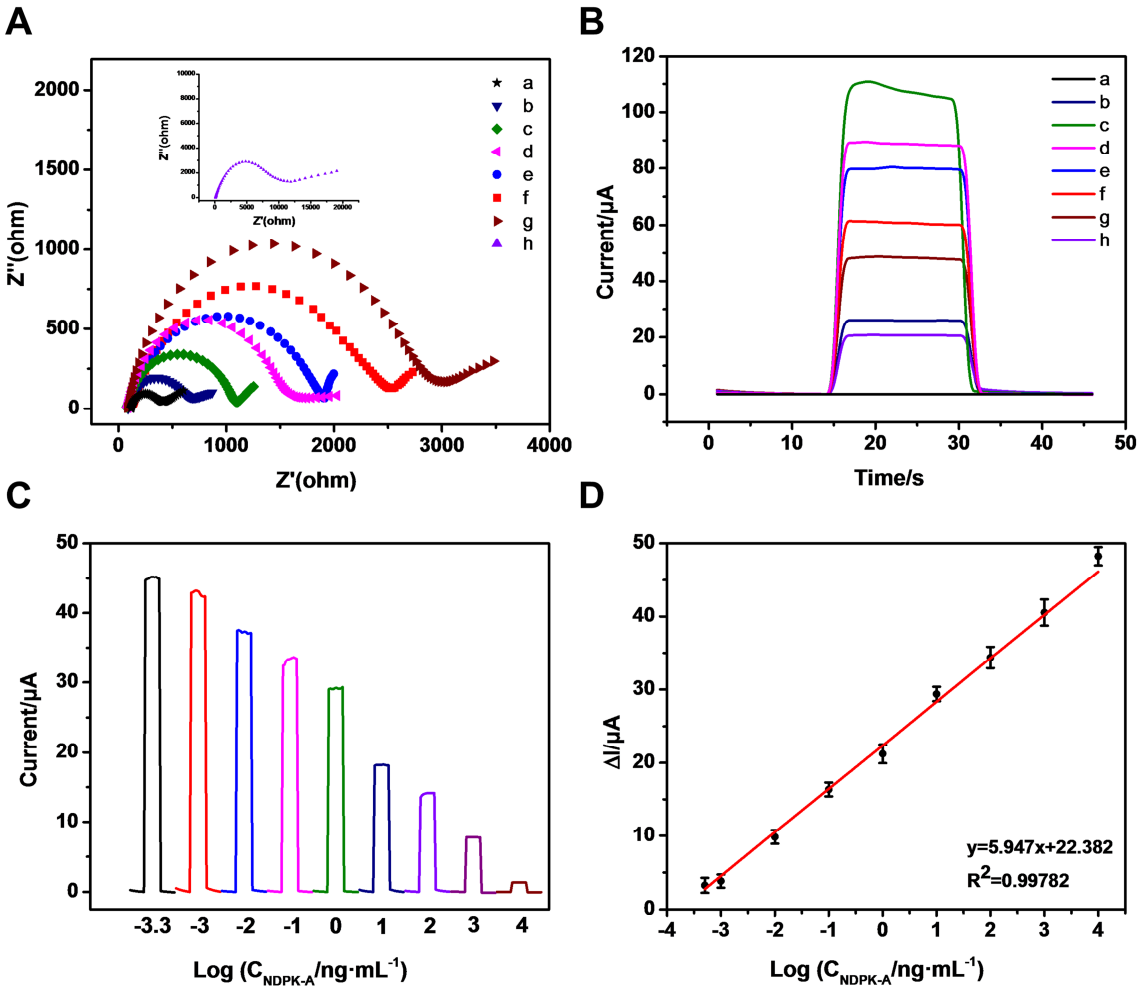
A
Z''(ohm)
Z'(ohm)
a
b
c
d
e
f
g
h
B
Current/μA
Time/s
C
Current/μA
Log (C_NDPK-A/ng·mL^-1)
D
ΔI/μA
y=5.947x+22.382
R^2=0.99782
Log (C_NDPK-A/ng·mL^-1)

ACCEPTED

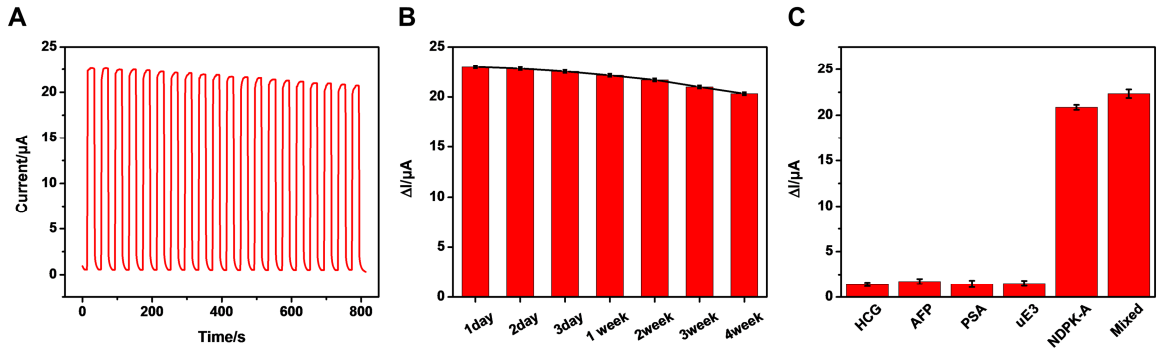

ACCEPTED MANUSCRIPT

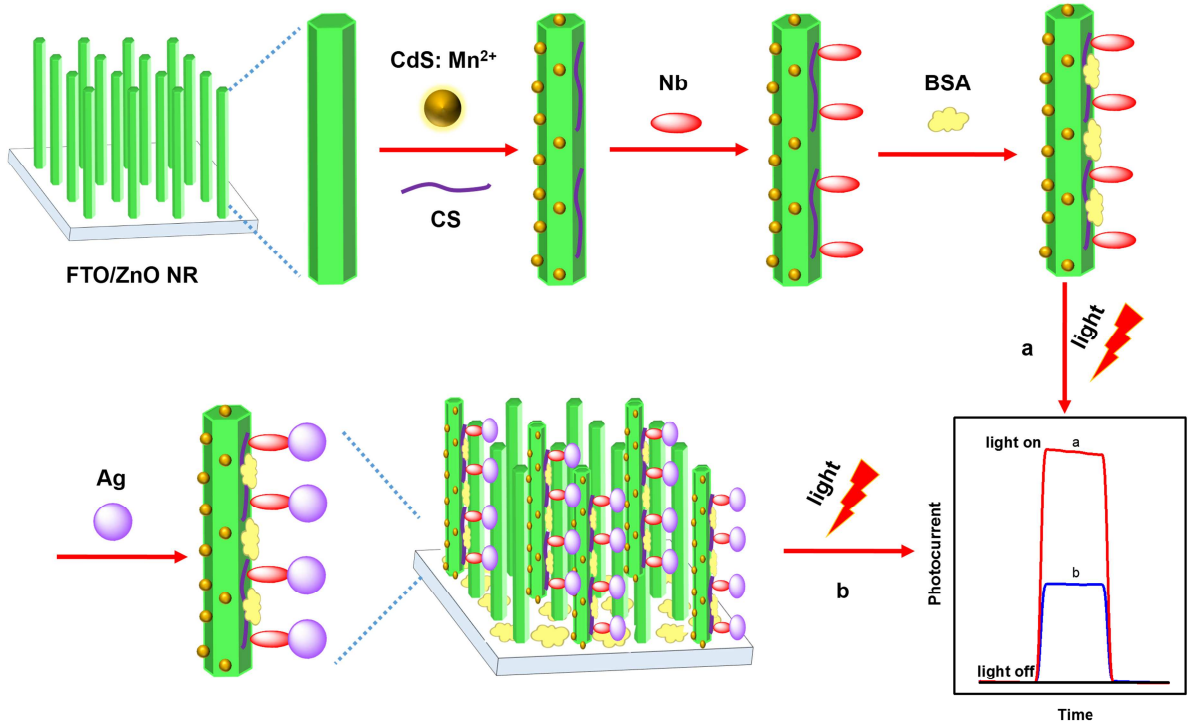

ACCEPTED MANUSCRIPT

ACCEPTED MANUSCRIPT

Highlights

- A photoelectrochenmical immunosensor based on ZnO NAs and NBs was fabricated
- Cosensitized structure of ZnO NAs, CdS and Mn improved the photocurrent response
- An excellent sensitivity and selectivity of NDPK-A detection was obtained

ACCEPTED MANUSCRIPT